JACS
JOURNAL OF THE AMERICAN CHEMICAL SOCIETY
Article
pubs.acs.org/JACS

Mechanical Transition from α-Helical Coiled Coils to β-Sheets in Fibrin(ogen)

Artem Zhmurov,[†,‡] Olga Kononova,[†,‡] Rustem I. Litvinov,[§] Ruxandra I. Dima,[∥] Valeri Barsegov,*[,†,‡] and John W. Weisel*[,§]

[†]Department of Chemistry, University of Massachusetts, Lowell, Massachusetts 01854, United States

[‡]Moscow Institute of Physics and Technology, Moscow Region, Russia 141700

[§]Department of Cell and Developmental Biology, Perelman School of Medicine, University of Pennsylvania, Philadelphia, Pennsylvania 19104, United States

[∥]Department of Chemistry, University of Cincinnati, Cincinnati, Ohio 45221, United States

Supporting Information

ABSTRACT: We characterized the α-to-β transition in α-helical coiled-coil connectors of the human fibrin(ogen) molecule using biomolecular simulations of their forced elongation and theoretical modeling. The force (F)−extension (X) profiles show three distinct regimes: (1) the elastic regime, in which the coiled coils act as entropic springs (F < 100−125 pN; X < 7−8 nm); (2) the constant-force plastic regime, characterized by a force-plateau (F ≈ 150 pN; X ≈ 10−35 nm); and (3) the nonlinear regime (F > 175−200 pN; X > 40−50 nm). In the plastic regime, the three-stranded α-helices undergo a noncooperative phase transition to form parallel three-stranded β-sheets. The critical extension of the α-helices is 0.25 nm, and the energy difference between the α-helices and β-sheets is 4.9 kcal/mol per helical pitch. The soft α-to-β phase transition in coiled coils might be a universal mechanism underlying mechanical properties of filamentous α-helical proteins.

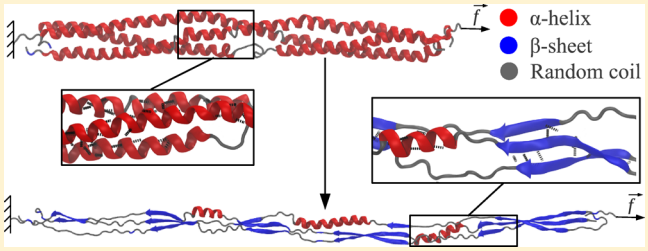

Large structural transitions constitute an essential mechanism of protein function and dysfunction, including folding, unfolding, and misfolding, conformational activation and inactivation, aggregation, protein−protein interactions, etc. Secondary structure alterations, including the α-helix to β-sheet (α-to-β) transition, have been suggested as a universal mechanism of protein unfolding.[1−4] It has been shown experimentally[5−8] and theoretically[9−11] that upon mechanical unfolding, protein polymers containing two-stranded α-helical coiled coils, such as α-keratin,[7] α-keratin-like intermediate filaments,[8] wool fibers,[5] vimentin,[11] and desmin intermediate filaments,[6] form structures with β-sheet architecture. In the α-helical coiled coil, two or more right-handed α-helices wind around each other to form a left-handed supercoil.[12] Fibrin is another protein polymer containing relatively large but three-stranded α-helical coiled coils that could undergo the α-to-β phase transition, which is directly related to the deformability of fibrin that underlies its vitally important functions.

Fibrin polymers form in the blood at sites of vascular injury and provide the scaffold for hemostatic plugs and pathological thrombi that block blood vessels. Fibrin is formed from fibrinogen, a 340 kDa dimeric blood plasma protein consisting of three pairs of Aα, Bβ, and γ chains linked by S−S bonds.[13,14] Two distal parts and one central globular part of fibrinogen are connected by two 17 nm long three-stranded α-helical coiled coils (Figure 1). Fibrin formation is initiated by the enzymatic cleavage of fibrinopeptides A and B from the N-termini of the Aα and Bβ chains, respectively, converting fibrinogen to fibrin monomer (containing α, β, and γ chains), which maintains major structural features of fibrinogen. Monomeric fibrin self-assembles, resulting in a filamentous network that is stabilized by covalent cross-linking.[15]

Structural changes underlying the critically important mechanical properties of fibrin have been found to occur on different spatial scales.[16] At the molecular level, the response to fibrin clot stretching represents forced unfolding of structural domains,[16,17] but there is disagreement regarding the particular structures of fibrin(ogen) (Fg) involved.[16−20] Our recent work utilizing atomic force microscopy-based single-molecule unfolding and pulling simulations has shown that mechanical unraveling of Fg is determined by the coupled stepwise unfolding of the globular γ-nodules and reversible extension−contraction of the coiled-coil connectors.[21]

It has been hypothesized that molecular extension of fibrin is accompanied by the α-to-β conversion of the coiled coils.[18] By means of Congo red staining, which is commonly used to identify stacks of β-sheets in amyloid proteins, the formation of a congophilic material in stretched fibrin fibers (presumably new β-sheets) was revealed,[17] although the specificity of this

Received: August 7, 2012
Published: September 6, 2012

   dx.doi.org/10.1021/ja3076428 | J. Am. Chem. Soc. 2012, 134, 20396−20402

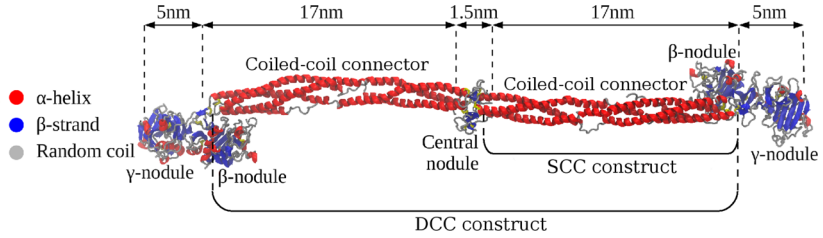

Figure 1. All-atom structure of human fibrinogen (PDB entry 3GHG) showing two coiled-coil connectors, the central nodule, γ-nodules, and β-nodules. Also shown are dimensions of the crystal structure of fibrin(ogen) (Fg), including the double three-stranded coiled coil (DCC) and single three-stranded coiled coil (SCC) constructs.

method is not fully justified. Direct experimental evidence for the α-to-β transition in stretched and compressed hydrated fibrin clots has recently been obtained using FTIR-spectroscopy.[22] Hence, given the immense biological importance of fibrin deformation and the lack of information about underlying molecular structural changes, monomeric Fg is a prime system for studying the mechanisms of the mechanical α-to-β transition in fibrin and other α-helical proteins.

We present the results of our theoretical and computational exploration of the mechanism of forced elongation of the Fg molecule and its portions, which include two symmetrical coiled coils connected by the central nodule [i.e., the double coiled coil (DCC); each of the coiled coils contains residues Aα27−200, Bβ58−197, and γ14−139] and a single coiled coil (SCC; residues Aα45−200, Bβ76−197, and γ19−139). Biomolecular simulations provide a detailed nanoscale picture of structural transitions in proteins.[23,24] However, because of the very large system size (from 500 amino acid residues for the SCC portion to 2868 residues for the full-length Fg molecule), theoretical modeling of Fg remains challenging. We utilized all-atom molecular dynamics (MD) simulations implemented on graphics processing units (GPUs) to speed up the simulations.[25,26]

Our results show that the force-induced molecular elongation of Fg is determined by the dynamic interplay between unwinding/extension of the α-helical coiled coils and unfolding of the γ-chain nodules. The mechanical response of the coiled-coil connectors shows a remarkable α-to-β structural transition to form elongated three-stranded parallel β-sheets. The force-induced structural rearrangements described at the nanoscale provide a molecular basis for understanding the unique physical properties of fibrin fibers, including their extensibility, viscoelasticity, and strain hardening.[27]

RESULTS

We carried out pulling simulations for the SCC and DCC portions of Fg and for the full-length Fg molecule without flexible αC regions and N-termini of the Aα, Bβ, and γ chains that are unresolved in the crystal structure [Figure 1; also see the Supporting Information (SI)]. We employed a time-dependent (ramped) force $f(t) = r_f t$ (where r_f is the force loading rate) to study the dependence of the unfolding force F (i.e., the mechanical response) on the molecular extension X, and we used a force-clamp protocol to resolve the average extension $\langle X \rangle$ as a function of a constant tensile force f (see Methods). The former characteristic can be compared with experimental F−X curves of protein mechanical unfolding. The latter is a phase diagram to describe different regimes of the mechanical elongation. Because of the high complexity of the Fg molecule, we employed MD simulations in implicit water using the solvent-accessible surface area (SASA) and generalized Born (GB) models.[28−31]

Unfolding of Full-Length Fg. We first studied forced elongation of full-length Fg. The sawtoothlike F−X profiles for Fg capture multistep sequential unfolding transitions that occur in the symmetric left and right γ-nodules. These transitions give rise to distinct 75−150 pN force peaks separated by a peak-to peak distance of 20−30 nm (Figure 2). These findings agree

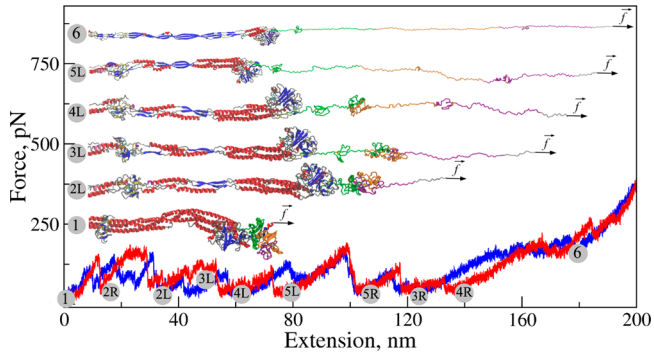

Figure 2. Force−extension curves (two independent trajectories shown in red and blue color) for unfolding of Fg (ramped force, SASA model; see Figure S1 in the SI). Also shown are structural snapshots for the folded state (structure 1), transient conformations (2L−5L), and the unfolded state (6) for the left (L) half of the Fg molecule, which correspond to different stages of unfolding (force peaks). The labels 2R−5R in the force−distance curves indicate similar transitions observed in the symmetric right (R) half of the molecule. The force was applied along the end-to-end vector connecting the constrained and tagged residues in the γ chains. The C-terminal domain, the central domain, and the N-terminal domain are shown in purple, orange, and green, respectively.

well with our previous results from coarse-grained modeling of forced Fg unfolding.[21] The first two force signals are due to the β-strand (residues γ379−395) pull-out (structures 2R and 2L). The next three force signals correspond to unfolding transitions in the left γ-nodule (structures 3L−5L): first, unfolding of the C-terminal part of the γ-nodule (residues γ309−326 and γ339−379) occurs, giving structure 3L (a transition of type 2 described previously[21]); second, the central domain of the γ-nodule (residues γ219−309) unfolds, giving structure 4L (a transition of type 1[21]); third, unfolding of the N-terminal domain of the γ-nodule (residues γ139−153 and γ182−219) occurs, giving structure 5L (a transition of type 3[21]). The remaining three force peaks correspond to the same unfolding transitions in the right γ-nodule (structures 5R, 3R, and 4R; Figure S1 in the SI). The mechanical elongation of the coiled coils does not result in detectable force signals.

dx.doi.org/10.1021/ja3076428 | J. Am. Chem. Soc. 2012, 134, 20396−20402

Unfolding of the DCC Connectors. To characterize the unfolding of the coiled-coil connectors, we carried out pulling simulations for the DCC portion of the Fg molecule without globular β- and γ-nodules (see Methods). The F–X profiles have three distinct regimes (Figure 3 and Table 1). At lower forces (<100–125 pN), the unfolding force F grows linearly with X (i.e. $F \sim X$; Figure 3). In this linear regime, starting from the twisted state (structure 1 in Figure 3), the coiled coils unwind by a large angle $\theta = 2\pi$ (Table 1) while responding elastically to the applied force (structure 2). We observed the formation of transient short β-strands ("β-seeds") comprising 4–6 amino acid residues and random coils in the least structured parts of the Aα chain (Aα88–102), Bβ chain (Bβ133–142), and γ chain (γ66–84). We calculated the apparent spring constant for the DCC construct in the linear regime by taking the derivative of F with respect to X and found $dF/dX \approx 33$ pN/nm. To study the reversibility of the elastic transitions, we performed refolding simulations for the DCC construct using the structures stretched by 3 and 7 nm as the initial states (see Methods). All of the simulation runs showed full refolding; the force–retraction curves closely follow the F–X curves, and the hysteresis is small (Figure 3).

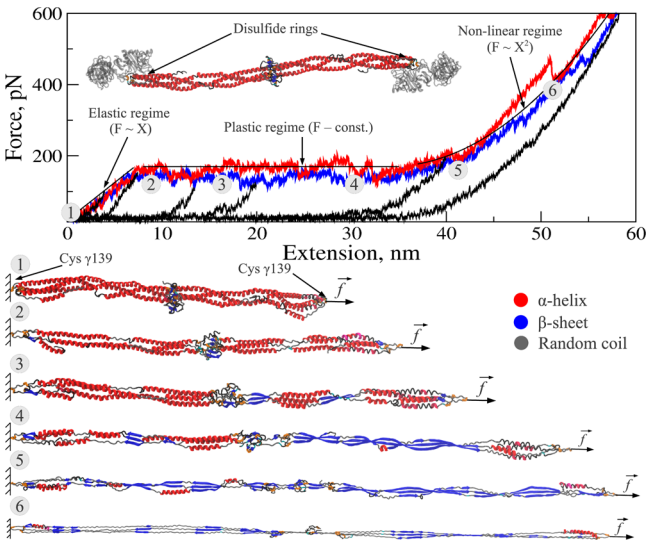

Figure 3. Force–extension curves (two independent trajectories shown in red and blue color) for the DCC portion of Fg (ramped force, SASA model; see Figure S2 in the SI). The force was applied along the end-to-end vector connecting Cys γ139 in the left and right coiled coils (structure 1). Also shown are the snapshots for the folded state (structure 1), transient conformations (2–5), and the unfolded state (6). The force–retraction curves (black) represent refolding simulations; we used stretched conformations extended by 3 and 7 nm (linear regime), 13 and 21 nm (constant-force regime), and 40 and 60 nm (nonlinear regime) as initial states.

The linear regime persists until X = 7–8 nm. Beyond this point, the unfolding force levels off, reaching a long plateau at F = 150 pN. In this constant-force regime, the coiled coils extend to 35–40 nm (Figure 3), that is, they behave as a plastic material. The Aα, Bβ, and γ chains quickly rewind, undergoing the reverse -2π rotation around the pulling axis to form the initial twisted state. Significantly, the three-stranded α-helices are gradually transformed into three-stranded parallel β-sheets (Figure 3). The dynamics of the structural transitions in the DCC construct, in terms of the propensity to form α-helices or β-strands, is presented in Figure S2 in the SI. Ramachandran plots of the dihedral angles ϕ and ψ, which are sensitive to changes in the secondary structure of proteins (Figure S3 in the SI), show that ϕ and ψ move from the α-helical region ($-90° < \phi < -30°$ and $-60° < \psi < 0°$) to the β-structure region ($-180° < \phi < -60°$ and $90° < \psi < 180°$) through the transition region with mixed $\alpha + \beta$ character ($-100° < \phi < -75°$ and $0° < \psi < 90°$).

When the α-to-β transition set in, we witnessed the formation of exotic, spiral segments of the three-stranded parallel β-sheets (Figure 3, structure 4), which unfold and unwind simultaneously (compare, e.g., structures 4 and 5). The coupled unfolding–unwinding transition starts from the least structured central part of the coiled coils and involves ~90% of the residues in the Aα, Bβ, and γ chains (structure 3). Because of tension fluctuations, transient π-helical and 3_{10}-helical structures form (not shown). At $X \approx 40$ nm, almost all of the α-helical segments are converted into β-sheets (structure 5). Because the potential energy of the chain does not change upon unwinding, $+2\pi$ unwinding (-2π rewinding) in the linear (constant-force) regime corresponds to entropic contributions to the molecular extension (contraction). To examine the reversibility of unfolding in the constant-force regime, we carried out refolding simulations for the DCC construct using partially unfolded structures stretched by 13 and 21 nm. We found the force–retraction curves to deviate notably from the F–X curves, with large hysteresis (Figure 3). None of the simulation runs showed full refolding to the initial folded state in the 2 μs time period.

At X = 35–40 nm, the unfolding force F starts to increase again, marking the beginning of the nonlinear regime (Figure 3). Here an elongation of the coiled coils to $X \approx 55$–60 nm is accompanied by a parabolic increase in the unfolding force (i.e., $F \sim X^2$; Figure 3, structure 6). This regime corresponds to excitation of the bond angles (straightening of the protein backbone), which is reflected in an unusually steep rise of F to 700 pN combined with a moderate 10 nm increase in X to 60 nm (Figure 3). The unwinding angle is close to zero (Table 1) since the Aα, Bβ, and γ chains are fully extended (structure 6).

Table 1. Three Regimes of the Mechanical Response of the DCC and SCC Portions of Fg to External Physical Factors, Classified in Terms of the Molecular Extension (X), the Unwinding (Rewinding) Angle (θ), and the Unfolding Force (F), and Summary Descriptions of Their Elongation Mechanisms

	X (nm)		θ (rad)		F (pN)		
regime	DCC	SCC	DCC	SCC	DCC	SCC	mechanism
linear (elastic) regime	<7–8	<2–3	$+2\pi$	$+\pi$	<100–125	<100	unwinding of coiled coils; formation of "seeds" of β-strands
constant-force (plastic) regime	~8–35	~4–17	-2π ($+2\pi$)	$-\pi$ ($+\pi$)	150	100–200	rewinding, elongation, and re-unwinding of parallel β-sheets
nonlinear regime	40–60	18–21	~0	~0	>175–200	>200	full elongation; formation of long β-sheets

dx.doi.org/10.1021/ja3076428 | J. Am. Chem. Soc. 2012, 134, 20396–20402

A small variation in F at $X \approx 50-55$ nm is due to unfolding of the central nodule (structure 6), which occurs only after all of the coiled coils have been unwound, fully stretched, and converted to β-sheets. Refolding simulations for the DCC construct in the nonlinear regime starting from the structures stretched by 40 and 60 nm did not show any refolding (Figure 3).

Mechanism of the α-to-β Phase Transition. To model the α-to-β phase transition in the coiled coils, we carried out force-clamp simulations (see Methods) for the SCC portion of Fg. The profiles of the average total extension of the SCC construct, $\langle X \rangle$, as a function of the tensile force f are sigmoidal (S-shaped) (Figure 4). In the low-force regime (<100 pN) and high-force regime (>200 pN), which correspond mostly to pure α-helices and β-structures, respectively, the molecular extension is very small. In the 100–200 pN transition range, the SCC construct undergoes a remarkable 15 nm elongation from ~3 to ~18 nm (Figure 4). Here, the α-helical coiled coils unwind and are transformed into three-stranded parallel β-sheets (Figure 4). The α-helical content decreases while the share of β-strands increases with increasing pulling force.

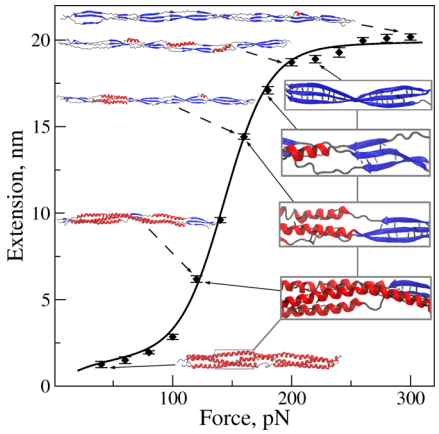

Figure 4. The α-to-β phase transition in the Fg coiled coils (SASA model; see Figure S3 in the SI), as reflected in the S-shaped profile of the average extension $\langle X \rangle$ (with standard deviations) vs constant force f. The theoretical curve $X(f)$ (solid line) was used to fit the unfolding data points. Also shown are snapshots of the α-state, the β-state, and the transition state (mixed $\alpha + \beta$ character) as well as the network of intramolecular hydrogen bonds in the α-state (in the Aα, Bβ, and γ chains), intra- and intermolecular hydrogen bonds in the transition state (in the chains and between β-strands), and intermolecular hydrogen bonds in the β-state (between β-strands).

The mechanisms of the α-to-β transition in the SCC and DCC constructs are similar (Table 1). The low-force regime, transition regime, and high-force regime observed in the force-clamp simulations (f - constant; Figure 4) correspond to the linear, constant-force, and nonlinear regimes of mechanical elongation in the ramped force [$f(t) = r_f t$] simulations (Figure 3). We analyzed the propensities of the coiled coils to form α-helices and β-strands as a function of pulling force (Figure S3 in the SI). These can be viewed as the force-dependent populations of the α-helices and β-structures [$p_\alpha(f)$ and $p_\beta(f)$, respectively]. At low forces, ~90% of the DCC (or SCC) structure is α-helical, whereas the percentage of β-strands is zero. Hence, in the folded state, ~10% of the coiled-coil connectors contain random coils. When $f > 200-300$ pN, the percentage of α-helices drops to zero and that of β-strands rises to 90%. In the fully unfolded state, the same residues remain in the random-coil conformation (~10% of the chains). Although the number of hydrogen bonds in the DCC construct decreases from 375 to 200 in the 0–300 pN force range (Figure S3 in the SI), it does not reach zero even at the highest forces (f = 500–600 pN) because the nascent β-sheet structure is stabilized by the transverse (interchain) hydrogen bonds.

We analyzed the phase diagram shown in Figure 4 using a two-state model (see Methods) in which the SCC is partitioned into the "α-state" (for α-helical coiled coils) and the "β-state" (for three-stranded β-sheets). Because of the linear regime ($F \sim X$) observed at low forces (Figure 3), we modeled the α-state as an entropic spring. The β-state was described by a wormlike chain.[32,33] Force application induces molecular elongation in the α- and β-states and lowers the energy barrier for the α-to-β transition (see Methods). The total extension $X(f)$ is the superposition of the extensions: $X(f) = p_\alpha(f)y_\alpha(f)L_\alpha + p_\beta(f)y_\beta(f)L_\beta$, where p_α and p_β are the populations, y_α and y_β the fractional extensions, and L_α and L_β the total (maximal) extensions for the α- and β-states, respectively. We performed a fit of the simulated data points for the SCC construct using the theoretical curve of $X(f)$ and obtained a very good match (Figure 4). We found that the spring constant is k_α = 35.1 pN/nm and the maximum extension is L_α = 4.4 nm for the α-state. For the β-state, the persistence length is l_β = 1.5 nm and the maximum extension (contour length) is L_β = 19.7 nm. The equilibrium distance between the α-state and the transition state is $z_{\alpha\beta}$ = 0.25 nm, and the free energy difference separating the α- and β-states is ΔG_0 = 4.9 kcal/mol per helical pitch.

DISCUSSION

We have performed an in-depth computational and theoretical study of the fibrin(ogen) nanomechanics. To separate the contributions to molecular elongation from the coiled-coil connectors of Fg, we performed pulling simulations for the double three-stranded coiled coil (DCC) and single three-stranded coiled coil (SCC) portions of Fg. These mimic the ramp-force and force-clamp modes used in experimental forced protein unfolding assays. Because of the very large number of degrees of freedom, we used implicit solvation models. To exclude possible model-dependent artifacts, we adopted the SASA and GB models, which are based on different approaches to solvation effects.

Verification of the simulation approach used in this study was provided by the fact that the mechanism of unfolding of the γ-nodules observed in all-atom detail was quite similar to the one described in our coarse-grained modeling study.[21] A minor difference was that in the all-atom modeling the C-terminal β-strand "pull-out" from the γ-nodule did not always lead to its immediate dissociation into the C-terminal and N-terminal domains. The binding contacts at the interface of the C- and N-terminal domains in the γ-nodule stabilize the structure, but only for a short period of time. Hence, the C-terminal β-strand "pull-out" and unraveling of the central domain (transition of type 1)[21] might occur in two steps. However, because of the stochastic nature of the protein mechanical unfolding, both scenarios are possible. Our data are consistent with the calorimetric study, which showed that the removal of the C-terminal β-strand renders the γ-nodule less stable.[34]

A previous study[23] attempted to resolve the molecular mechanism of Fg unfolding. Because of the large number of degrees of freedom (1 018 000 atoms), those authors used a pulling speed that was 25 times higher than the one used here.

dx.doi.org/10.1021/ja3076428 | J. Am. Chem. Soc. 2012, 134, 20396–20402

We were able to utilize a lower pulling speed and follow fewer degrees of freedom because we utilized implicit water models, which have been used in theoretical studies of forced protein unfolding,[9,11] and GPU computing. The point of force application used in ref 23 was different from ours; we applied the pulling force to the last crystallographically resolved residue in the γ-nodule, which corresponds to the covalent $\gamma-\gamma$ cross-linking site. In spite of the differences in methodology, the $F-X$ profiles for the Fg coiled coils presented here and in ref 23 are very similar.

The $F-X$ profiles for the DCC portion of Fg show three distinct regimes (Figure 3). In the linear regime, the system responds elastically to the pulling force, whereas in the constant-force regime (with a force plateau) the molecule behaves as a plastic material. Molecular elongation of the coiled coils continues in the nonlinear regime, where force performs work against the bond angles and dihedral angles. A similar shape of the $F-X$ profiles with three distinct regimes was observed for myosin double-helical coiled coils, albeit at lower forces (30−40 pN).[35] Remarkably, when forced unfolding of coiled coils occurs concomitantly with unfolding of the globular domains, as in the case of Fg monomer, the force peaks due to abrupt unraveling of the globular structures overlap and mask the force plateau due to unfolding of the coiled coils (Figure 2 and ref 36).

In the linear (elastic) regime, elongation of the coiled coils is due to their unwinding around the uniaxial direction of the pulling force (the coiled coil extends as a whole, but the Aα, Bβ, and γ chains do not elongate). The potential energy (enthalpy) of the coiled-coil connectors remains constant ($\Delta H_{el} \approx 0$; data not shown), so the Gibbs energy change (ΔG_{el}) is due to the entropy change (i.e., $\Delta G_{el} \approx -T\Delta S_{el}$). Hence, in the elastic regime, the Fg coiled coils act as an entropic spring. For the SCC construct, $T\Delta S_{el} \approx -90$ kJ/mol. This is about a half of the $T\Delta S$ value of −201 kJ/mol for unfolding of the two coiled coils from our earlier study,[21] indicating good agreement between these results and our previous estimates. In the linear regime, the coupled elongation and unwinding are fully reversible (Figure 3). In the constant-force (plastic) regime, the forced elongation of the coiled coils is driven by the change in the internal energy. For the DCC construct, $\Delta H_{pl} \approx 330$ kJ/mol, which is comparable to the ΔH value of 285 kJ/mol for complete unfolding of two coiled coils from our earlier study.[21] In the constant-force regime, the coiled coils contract and rewind but only partially refold. In the nonlinear regime, when the pulling force is quenched, the coiled coils contract but remain in the random-coil configuration. Hence, the three regimes are different with respect to the unfolding reversibility: unfolding is fully reversible in the linear (elastic) regime, partially reversible in the constant-force (plastic) regime, and irreversible in the nonlinear regime (in microsecond-time-scale simulations).

The broad 100−200 pN transition range in the phase diagram (Figure 4) reveals that the α-to-β transition is noncooperative (α-helical segments unravel independently). The estimated spring constant in the α-helical state, $k_\alpha = 35.1$ pN/nm, is close to the linear slope of 33 pN/nm from the $F-X$ profiles (Figure 3). The maximal extension of the α-helices, $L_\alpha = 4.4$ nm, is close to the extension of 3−4 nm for the "α-state" from the phase diagram (Figure 4). The long persistence length in the "β-state", $l_\beta = 1.5$ nm (corresponding to 4−5 residues), is reasonable given the planar extended structure of β-sheets. The unfolding forces for the DCC and SCC portions are considerably larger than the ∼50 pN forces required for unfolding of double-helical myosin coiled coils.[35] We ascribe this difference to the more mechanically resilient three-stranded coiled coils of the Fg molecule. The maximal extension of the β-sheets obtained, $L_\beta = 19.7$ nm, corresponds to the total extension $L_\alpha + L_\beta \approx 24$ nm observed at larger forces (>300 pN; data not shown).

The distance to the transition state for a helical pitch, $z_{\alpha\beta} = 0.25$ nm, is close to the published estimate of 0.12 nm[9] but shorter than the same quantity for the globular D regions (∼1 nm).[21] This indicates that α-helices are readily transformed into β-strands when the pulling force is high enough to change the dihedral angles. The force at which the α-to-β transition sets in is $f^* \approx 150$ pN (Figure 4), and the energy barrier is $\Delta G^{\ddagger} \approx f^* z_{\alpha\beta}/k_BT = 5.4$ kcal/mol. This is only slightly larger than the energy difference between the α-state and β-state at equilibrium, $\Delta G_0 \approx 4.9$ kcal/mol, which accounts for the disruption of one N−H···O hydrogen bond (∼3 kcal/mol)[37] and changing the dihedral angles (∼2 kcal/mol).[38] The difference between the length of the α-helical pitch ($x_\alpha \approx 0.54$ nm) and the contour length in the β-sheet for the ∼3.6 residues forming the pitch ($x_\beta \approx 1.3$ nm) is $\Delta x_{\alpha\beta} = x_\beta - x_\alpha \approx 0.75$ nm, from which we find that the distance between the β-state and the transition state for the reverse β-to-α transition is $z_{\beta\alpha} = \Delta x_{\alpha\beta} - z_{\alpha\beta} \approx 0.5$ nm.

The mechanical and rheological behavior of fibrin clots can be understood only by integration of their materials properties at the bulk, network, fiber, and molecular levels.[16] The mechanism of the α-to-β transition in fibrin upon forced elongation described here can explain some of the most unique features of fibrin polymers, such as strain hardening, viscoelasticity, and negative compressibility transitions.[27] The hypothetical α-to-β transition preceding the unfolding of the globular γ-nodules was estimated to account for up to 100% strain of fibrin fibers.[18] According to our new data (Figure 2 and ref 21), unfolding of the globular γ-nodules occurs before or concurrently with the α-to-β transition, but the contribution of the coiled coils to the overall extensibility should not depend on the order of unfolding events. This remarkable contribution is based on an elongation per residue from 0.15 nm in the α-helix to 0.32−0.34 nm in the β-strand. If the fraction of unfolded fibrin molecules reaches the maximum at a whole-clot macroscopic strain of ∼1.2,[17] then at this strain additional unfolding mechanisms must play a role. The first structure to unfold in Fg is the globular γ-nodule,[21] and unfolding of one γ-nodule with a contour length of 80 nm may account for about a 2-fold extension of a 45 nm long folded fibrin molecule. The additional unfolding mechanism at strains of ≥1.2 could involve unwinding/unfolding and the α-to-β transition in the coiled coils. Remarkably, this strain corresponds to a nonlinear increase in the clot stiffness (strain hardening), which can be explained by formation of the more mechanically resistant β-sheets.[9]

Both unwinding and unfolding of the coiled coils are necessary to account for the elastic and plastic properties of the fibrin clots, inasmuch as these structural transitions have both elastic (fully reversible) and inelastic (partially reversible) regimes as the strain increases (Figure 3). In agreement with these data, it has been shown that the force−stretch response of the network[17] and individual fibers[19] is partially reversible with some hysteresis, which increases with strain. Also, the α-to-β transition is followed by protein aggregation within and between fibrin fibers, which can be driven by newly formed

intermolecular β-sheets, shown earlier to promote formation of protein aggregates.[40] In turn, protein aggregation is followed by a reduction in the water-accessible surface area and water expulsion, which can underlie the volume shrinkage of fibrin clots in response to extension (negative compressibility transitions).[16,17]

Our results offer new mechanistic, structural, and thermodynamic insights into the complex dynamic behavior of stretched fibrin polymers and an understanding of the unique role of coiled coils in fibrous proteins. The dynamic transition from the elastic regime to the plastic regime in mechanical elongation of Fg coiled coils followed by the remarkable α-to-β phase transition might provide a molecular basis underlying the unique physical properties of fibrin networks. The characteristic plateau regions in the force spectra of filamentous proteins with high α-helical content, such as Fg, might serve as dynamic signatures for the α-to-β transition. The two-state model used here to map the free energy landscape provides a theoretical framework for describing the α-to-β transition in proteins. The unwinding of the Fg coiled coils indicates that the physical properties of proteins with α-helical coiled-coil structures are best understood in terms of the multidimensional energy landscape, where multiple coupled reaction coordinates characterize their unfolding nanomechanics.

METHODS

Pulling Simulations. We performed all-atom MD simulations implemented on a GPU using the structural models of the whole human Fg molecule and the DCC and SCC portions described in the SI. We employed the SASA and GB models[39,28−31] of implicit solvation (see the SI).

Ramped-Force Simulations. To imitate the experimental ramped-force measurements for the Fg and DCC systems, we constrained one end of the molecule and applied a time-dependent force $\mathbf{f}(t) = f(t)\mathbf{n}$ to the other in the direction $\mathbf{n}$ parallel to the end-to-end vector. The constrained and pulled residues were γ394 and symmetrical γ395 for Fg and γ139 and symmetrical γ139 for DCC, respectively. The force amplitude $f(t) = r_f t$ was increased linearly with the loading rate $r_f = k_{sp}v_f$, where k_{sp} = 100 pN/nm is the spring constant and v_f is the pulling speed. The lowest pulling speed we could use to complete 2 μs runs in a reasonable "wall-clock" time (~48 days per trajectory) on a GPU (GeForce GTX 580) was $v_f = 10^5$ μm/s. In the simulations of force-quenched refolding, we used structures generated in the unfolding runs as initial states. The force $f(t) = f_0 - r_f t$ was decreased linearly at the same loading rate r_f starting from some initial value f_0.

Force-Clamp Simulations. For the SCC portion, we carried out pulling simulations using a constant force $\mathbf{f} = f\mathbf{n}$. The constrained and pulled positions were γ19 and symmetrical γ139, respectively. We generated five 2 μs runs for each force value to resolve the average extension $\langle X \rangle$ and fluctuations ΔX.

Two-State Model. The "α-state" was modeled as a harmonic spring with energy $G_\alpha = k_\alpha X_\alpha^2/2$, where k_α is the spring constant and $X_\alpha = f/k_\alpha$ is the average extension, and maximum extension L_α. The "β-state" was modeled by a wormlike chain[32,33] with bending energy $G_\beta = (3k_BT/2l_\beta) \int [\partial u(s)/\partial s]^2 \, ds$, where l_β is the persistence length, T is the absolute temperature, and k_B is Boltzmann's constant, and contour length (maximum extension) L_β. Because at $f = 0$ the free energies of the two states differ by an amount $\Delta G_0 = G_\beta - G_\alpha$ that is large compared with the thermal fluctuations (i.e., $\Delta G_0 \gg k_BT$), the molecule is in the α-state at $f = 0$. Application of a force stretches the molecule, which can be quantified by the fractional extension $y_\alpha(f) = X_\alpha(f)/L_\alpha$; this lowers the free energy barrier by an amount $fz_{\alpha\beta}$, giving $\Delta G(f) = \Delta G_0 - fz_{\alpha\beta}$, where $z_{\alpha\beta}$ is the distance from the minimum (α-state) to the transition state. For sufficiently high values of f, this leads to the α-to-β transition. The transition probability is given by the Boltzmann factor, $\exp[-\Delta G(f)/k_BT]$, which is equal to the ratio of the state populations, $p_\beta(f)/p_\alpha(f)$, where $p_\alpha + p_\beta = 1$. In the β-state, the molecule can be extended by an amount $y_\beta(f) = X_\beta(f)/L_\beta = 1 - \{\chi(t)^{1/3} + [(4/3)t - 1]/\chi(t)^{1/3}\}^{-1}$, where $\chi(t) = 2 + \{4 - [(4/3)t - 1]^3\}^{1/2}$ and $t = fl_\beta/k_BT$.

ASSOCIATED CONTENT

Supporting Information

Structural snapshots for Fg unfolding and detailed information about the secondary structure content, including Ramachandran plots and the populations of the α-helices and β-sheets. This material is available free of charge via the Internet at http://pubs.acs.org.

AUTHOR INFORMATION

Corresponding Author

Valeri_Barsegov@uml.edu; weisel@mail.med.upenn.edu

Notes

The authors declare no competing financial interest.

ACKNOWLEDGMENTS

This work was supported by the American Heart Association (Grant 09SDG2460023 to V.B.), the Russian Ministry of Education and Science (Grant 14.A18.21.1239 to V.B.), the National Institutes of Health (Grants HL030954 and HL090774 to J.W.W.), and the National Science Foundation (Grant MCB-0845002 to R.I.D.).

REFERENCES

(1) Takahashi, Y.; Ueno, A.; Mihara, H. *Structure* **2000**, *8*, 915−925.
(2) Sethuraman, A.; Vedantham, G.; Imoto, T.; Przybycien, T.; Belfort, G. *Proteins* **2004**, *56*, 669−678.
(3) Sethuraman, A.; Belfort, G. *Biophys. J.* **2005**, *88*, 1322−1333.
(4) Buehler, M. J.; Yung, Y. C. *Nat. Mater.* **2009**, *8*, 175−188.
(5) Church, J. S.; Corino, G. L.; Woodhead, A. L. *J. Mol. Struct.* **1998**, *440*, 15−23.
(6) Kreplak, L.; Herrmann, H.; Aebi, U. *Biophys. J.* **2008**, *94*, 2790−2799.
(7) Kreplak, L.; Doucet, J.; Dumas, P.; Briki, F. *Biophys. J.* **2004**, *87*, 640−647.
(8) Fudge, D. S.; Gardner, K. H.; Forsyth, V. T.; Riekel, C.; Gosline, J. M. *Biophys. J.* **2003**, *85*, 2015−2027.
(9) Qin, Z.; Buehler, M. J. *Phys. Rev. Lett.* **2010**, *104*, No. 198304.
(10) Daidone, I.; Simona, F.; Roccatano, D.; Broglia, R. A.; Tiana, G.; Colombo, G.; Di Nola, A. *Proteins* **2004**, *57*, 198−204.
(11) Qin, Z.; Kreplak, L.; Buehler, M. J. *PLoS One* **2009**, *4*, No. e7294.
(12) Cohen, C.; Parry, D. A. D. *Proteins* **1990**, *7*, 1−15.
(13) Brown, J. H.; Volkmann, N.; Jun, G.; Henschen-Edman, A. H.; Cohen, C. *Proc. Natl. Acad. Sci. U.S.A.* **2000**, *97*, 85−90.
(14) Spraggon, G.; Everse, S. J.; Doolittle, R. F. *Nature* **1997**, *389*, 455−462.
(15) Weisel, J. W. *Adv. Protein Chem.* **2005**, *70*, 247−299.
(16) Brown, A. E. X.; Litvinov, R. I.; Discher, D. E.; Purohit, P. K.; Weisel, J. W. *Science* **2009**, *325*, 741−744.
(17) Purohit, P. K.; Litvinov, R. I.; Brown, A. E. X.; Discher, D. E.; Weisel, J. W. *Acta Biomater.* **2011**, *7*, 2374−2383.
(18) Guthold, M.; Liu, W.; Sparks, E. A.; Jawerth, L. M.; Peng, L.; Falvo, M.; Superfine, R.; Hantgan, R. R.; Lord, S. T. *Cell Biochem. Biophys.* **2007**, *49*, 165−181.
(19) Liu, W.; Carlisle, C. R.; Sparks, E. A.; Guthhold, M. *J. Thromb. Haemostasis* **2010**, *8*, 1030−1036.
(20) Falvo, M. R.; Gorkun, O. V.; Lord, S. T. *Biophys. Chem.* **2010**, *152*, 15−20.
(21) Zhmurov, A.; Brown, A. E. X.; Litvinov, R. I.; Dima, R. I.; Weisel, J. W.; Barsegov, V. *Structure* **2011**, *19*, 1615−1624.
(22) Litvinov, R. I.; Faizullin, D. A.; Zuev, Y. F.; Weisel, J. W. *Biophys. J.* **2012**, *103*, 1020−1027.

(23) Lim, B. B. C.; Lee, E. H.; Sotomayor, M.; Schulten, K. *Structure* **2008**, *16*, 449−4596.
(24) Dima, R. I.; Joshi, H. *Proc. Natl. Acad. Sci. U.S.A.* **2008**, *105*, 15743−15748.
(25) Zhmurov, A.; Dima, R. I.; Kholodov, Y.; Barsegov, V. *Proteins* **2010**, *78*, 2984−2999.
(26) Zhmurov, A.; Rybnikov, K.; Kholodov, Y.; Barsegov, V. *J. Phys. Chem. B* **2011**, *115*, 5278−5288.
(27) Weisel, J. W. *Biophys. Chem.* **2004**, *112*, 267−276.
(28) Fraternali, F.; van Gunsteren, W. F. *J. Mol. Biol.* **1996**, *256*, 939−948.
(29) Eisenberg, D.; McLachlan, A. D. *Nature* **1986**, *319*, 199−203.
(30) Still, W. C.; Tempczyk, A.; Hawley, R. C.; Hendrickson, T. *J. Am. Chem. Soc.* **1990**, *112*, 6127−6129.
(31) Qiu, D.; Shenkin, P. S.; Hollinger, F. P.; Still, W. C. *J. Phys. Chem. A* **1997**, *101*, 3005−3014.
(32) Bustamante, C.; Marko, J. F.; Siggia, E. D.; Smith, S. *Science* **1994**, *256*, 1599−1600.
(33) Rief, M.; Fernandez, J. M.; Gaub, H. E. *Phys. Rev. Lett.* **1998**, *81*, 4764−4767.
(34) Yakovlev, S.; Loukinov, D.; Medved, L. *Ann. N.Y. Acad. Sci.* **2001**, *936*, 122−124.
(35) Schwaiger, I.; Sattler, C.; Hostetter, D. R.; Rief, M. *Nat. Mater.* **2002**, *1*, 232−235.
(36) Brown, A. E. X.; Litvinov, R. I.; Discher, D. E.; Weisel, J. W. *Biophys. J.* **2007**, *92*, L39−L41.
(37) Gao, J.; Kelly, J. W. *Protein Sci.* **2008**, *17*, 1096−1101.
(38) Pettitt, B. M.; Karplus, M. *J. Phys. Chem.* **1988**, *92*, 3994−3997.
(39) Ferrara, P.; Apostolakis, J.; Caflisch, A. *Proteins* **2002**, *46*, 24−33.
(40) Militello, V.; Casarino, C.; Emanuele, A.; Giostra, A.; Pullara, F.; Leone, M. *Biophys. Chem.* **2004**, *107*, 175−187.